Research Article GU J Sci, Part A, 12(1): 250-267 (2025) 10.54287/gujsa.1592619

Gazi University
Journal of Science
PART A: ENGINEERING AND INNOVATION
http://dergipark.org.tr/gujsa

Geochemical and Mineralogical Differentiation of Tepekent Basalts: A Multivariate Analysis Approach (NW of Konya-Central Anatolia)

Gülin GENCOGLU KORKMAZ[1*]

[1] *Konya Technical University, Engineering and Natural Sciences Faculty, Department of Geological Engineering, Türkiye*

Keywords

Basalt
Olivine
PCA
Pyroxene
Replenishment
UMAP

Abstract

This study investigates the mineralogical, petrographic, and geochemical characteristics of Miocene-aged basaltic rocks from the Tepekent region to distinguish and correlate them with other members of the Sulutus Volcanic Complex (SVC), particularly the Ulumuhsine and Yükselen basalts. Advanced geostatistical methods such as Principal Component Analysis (PCA), Uniform Manifold Approximation and Projection (UMAP), and k-medoids clustering analysis were applied to correlate the basaltic lava flows. While some overlaps were identified in whole-rock compositions, significant differences were observed in the mineral chemistry. The investigated basalts are primarily composed of plagioclase, with lesser amounts of olivine, pyroxene, and Fe-Ti oxides. Clinopyroxenes from the Tepekent basalts exhibit oscillatory zoning in MgO, CaO, Cr_2O_3, and TiO_2 contents, indicating magma recharge from a more mafic mantle source. Olivine phenocrysts show disequilibrium with their host magma but are in equilibrium with the most mafic Ulumuhsine basalt, suggesting they were derived from earlier solidified phases and subsequently incorporated into the system during magma ascent or convective processes within the magma chamber. Irregular An fluctuations and sieve textures in plagioclase crystals further support the presence of magma replenishment processes. Although isotopic data are indispensable in provenance studies to definitively identify magma sources and establish genetic relationships in greater detail, this study demonstrates how mineral chemistry and geostatistical analyses can effectively differentiate basaltic lava flows and elucidate complex magma chamber processes. The findings highlight the interplay between crustal contamination, mantle-derived magma replenishment, and multi-stage magmatic evolution, providing valuable insights into the volcanic history of Central Anatolia.

Cite

Gencoglu Korkmaz, G. (2025). Geochemical and Mineralogical Differentiation of Tepekent Basalts: A Multivariate Analysis Approach (NW of Konya-Central Anatolia). *GU J Sci, Part A, 12*(1), 250-267. doi:10.54287/gujsa.1592619

Author ID (ORCID Number)

0000-0003-0185-2806 Gülin GENCOGLU KORKMAZ

Article Process

Submission Date 28.11.2024
Revision Date 08.01.2025
Accepted Date 20.01.2025
Published Date 26.03.2025

1. INTRODUCTION

Subduction zone volcanism is characterized by multi-stage, multi-source, and multi-process magmatism, resulting in the formation and coexistence of magmas with diverse origins and compositions. The Late Mesozoic-Neogene geology of Turkey is closely linked to the opening and closure of the Neotethys Ocean (Şengör, 1979; Şengör & Yılmaz, 1981). In Central Anatolia, widespread Cenozoic volcanism is related to these tectonic events, with several volcanic provinces and complexes, such as the Galatia Volcanic Province (GVP), the Cappadocia Volcanic Province (CVP), the Sulutaş Volcanic Complex (SVC), the Erenlerdağ-Alacadağ Volcanic Complex (EAVC), the Karapınar Volcanic Field (KPVF), and the Karacadağ Volcanic Complex (KCVC), forming key geological features of the region (Şengör & Yılmaz, 1981; Aydar & Gourgaud,

*Corresponding Author, e-mail: ggkorkmaz@ktun.edu.tr

1998; Deniel et al., 1998; Uslular & Gençalioğlu-Kuşcu, 2019; Asan et al., 2021; Gençoğlu Korkmaz et al., 2022) (Figure 1).

The Sulutaş Volcanic Complex (SVC), located in the northwest of Konya, is part of the Neogene bimodal volcanic activity in Central Anatolia (Figure 1). It exhibits a diverse composition, including shoshonitic, calc-alkaline, high-K calc-alkaline, and Na-alkaline magmas. Bimodal volcanism, dominated by mafic and felsic products with the scarcity of intermediate compositions, reflects complex tectonic and magmatic processes. Previous studies have indicated that both crustal contamination and source enrichment played significant roles in the compositional diversity of the SVC (Gençoğlu Korkmaz et al., 2017; Asan et al., 2021). The SVC is situated within a graben-type extensional basin near Konya, bounded to the east by the Konya Fault Zone. This basin, filled with Neogene-aged sedimentary units, is underlain by Paleozoic and Mesozoic ophiolitic and metamorphic basement rocks. The extensional tectonics of the basin are linked to the rollback of a subduction zone associated with the Cyprus Arc, a result of the interaction between the African and Eurasian plates, which shaped the region's geodynamic evolution (Biryol et al., 2011; Delph et al., 2015; Gençoğlu Korkmaz et al., 2017). Neogene volcanic rocks, particularly dacitic and basaltic lava flows, are exposed in the east and west of the study area, and include enclaves of varying sizes. Dacites occur as lava flows and volcanic necks, while basalts form lava flows, cutting through pre-Neogene units (Gençoğlu Korkmaz et al., 2017).

Previous studies (Asan et al., 2021) yielded $^{40}Ar/^{39}Ar$ plateau and inverse isochron ages of 12.07 ± 0.06 Ma to 12.21 ± 0.32 Ma for the dacites and 11.01 ± 0.42 Ma to 11.05 ± 0.64 Ma for the calc-alkaline basalts in the Ulumuhsine-Küçükmuhsine region. On the other hand, a whole-rock sample from Yükselen basalts gave two plateau ages of 16.45 ± 0.76 Ma and 22.37 ± 0.65 Ma for the first and subsequent steps, respectively. These basalts are sodic alkaline, characterized by ocean island basalt (OIB)-like anorogenic geochemical signatures. Basaltic rocks with MgO > 4 wt% (Pecerillo, 2005) are key in deciphering mantle source compositions as they represent primary mantle-derived melts. Typically, basalts with elevated Cr (1000 ppm), Ni (400 ppm), and MgO (~8 wt%) contents reflect derivation from a primary mantle source (Weaver, 1991; Best, 2003). However, in the Tepekent region, the studied basaltic rocks show lower MgO, Cr, and Ni values, indicating they are highly evolved and not representative of primary mantle melts (Eryiğit et al., 2022). Despite this, their enriched nature allows them to be plotted on Nb/La-La/Yb and Zr/Y-Zr/Nb diagrams to assess degrees of melting and enrichment. Low Zr/Y (4.8-10.9) and Zr/Nb (8.11-15.29) values suggest partial melting of a lithospheric mantle source, with the enrichment likely due to subduction-related recycling of ancient oceanic crust (Eryiğit et al., 2022).

In this study, the Miocene-aged basaltic rocks from the Tepekent region are classified and correlated with those from Ulumuhsine and Yükselen, using mineral chemistry data and geostatistical methods (PCA, UMAP, K-means clustering). By examining clinopyroxene and olivine mineral chemistry, relationships between the lava flows are established and their magmatic evolution is discussed. This integrated approach provides a deeper understanding of the Tepekent basalts and contributes to the broader knowledge of the Sulutaş Volcanic

Complex, offering insights into the complex magmatic history of the Neogene volcanic activity in Central Anatolia.

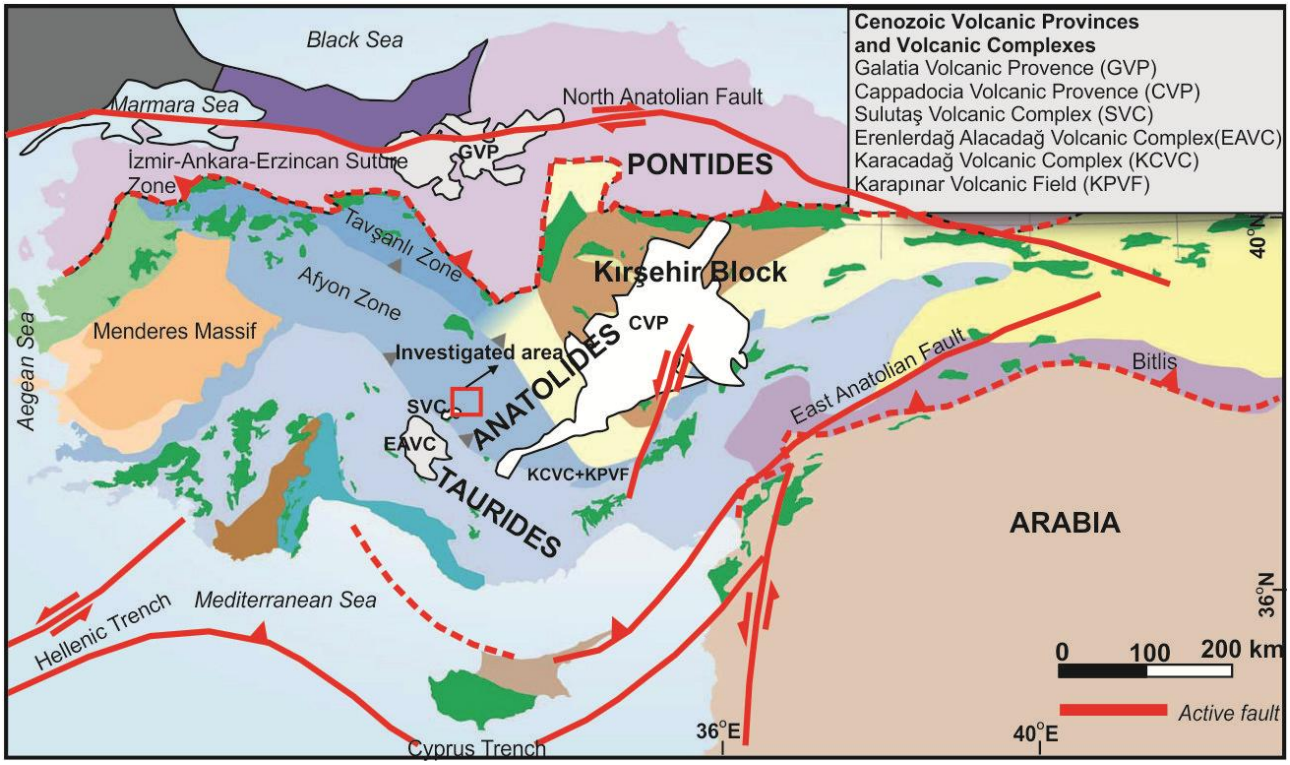

Figure 1. *Active tectonic map of Turkey showing Cenozoic Volcanic Provinces was modified from Van Hinsbergen et al. (2016). Map was taken from Gençoglu Korkmaz and Kurt (2024)*

2. MATERIAL AND METHOD

For petrographic and mineral chemistry analyses, approximately ten hand samples of basaltic rocks were collected from the Tepekent area (Konya, Central Anatolia). The sampling strategy was guided by whole-rock chemistry data published in Eryiğit et al. (2022). To strengthen the robustness of our analysis, additional data from the literature (Asan et al., 2021) were compiled and utilized for correlation and statistical evaluations.

Four carbon-coated, polished thin sections were prepared for mineral chemistry studies. The analyses were performed using a JEOL JXA-8600 electron microprobe at YEBIM (Ankara University), equipped with four wavelength-dispersive spectrometers (WDS) and an integrated energy-dispersive spectrometer (EDS) system. The operating parameters included a 20 nA beam current, 15 kV accelerating voltage, and a 20-second counting time per element. Detailed procedures for the analyses follow the methods described in Deniz and Kadıoğlu (2019). Structural formulae for pyroxenes were calculated based on four cations and six oxygens, for olivines based on four oxygens, while for feldspars, calculations were based on eight oxygens.

Thermobarometric conditions were determined using multiple methods. The clinopyroxene-liquid thermobarometers by Neave and Putirka (2017) and Putirka (2008a) and Lindsley and Andersen's (1983) pyroxene thermometer were employed for P-T estimations. The plagioclase thermobarometer (Putirka, 2008b)

was also applied to evaluate geothermal conditions. Equilibrium conditions for clinopyroxene-glass pairs and olivine-glass pairs were verified using the Kd(Fe-Mg) value of 0.27±0.03 (Putirka, 2008a) and 0.29±0.03 (Matzen et al., 2011; Putirka, 2016), respectively. WinPyrox and WinPLtb software (Yavuz, 2013; Yavuz & Yıldırım, 2018) were used for additional evaluations of hygrometric and depth conditions.

For geochemical interpretations, Igpet software (Carr, 1990) was utilized. Moreover, statistical analysis (Principal Component Analysis (PCA), Uniform Manifold Approximation and Projection (UMAP) and k-medoids analysis) were generated to assess geostatistical variations and to enhance the overall geochemical analysis.

3. RESULTS AND DISCUSSION

3.1. Results

Petrography and Mineral chemistry of the Tepekent basalts

The investigated basalts outcrop as lava flows in a very restricted area (Figure 2a and 2b) near Karardi Tepe (Tepekent region). They predominantly display holocrystalline porphyritic texture, with olivine and clinopyroxene as the dominant mafic mineral phases (Figure 2c-2f). The rocks consist of approximately 65% plagioclase, 15% olivine, 10% clinopyroxene, 5% sanidine and 5% opaque minerals (Figure 2c-2f). Zeolitization is observed locally within the basalts (Figure 2e). Olivines are predominantly occur as microphenocrysts, with rare occurrences of phenocrysts. In certain areas, fracture-filling and crack-filling structures are noted, along with iddingsite alteration along the crystal boundaries (Figure 2c-2f). Clinopyroxenes are primarily observed as microphenocrysts, while plagioclases are observed as both microlith and microphenocrysts.

In the studied basalts, the feldspar minerals are predominantly represented by labradorite, with rare occurrences of sanidine (Figure 3). While plagioclases are primarily labradorite, their rims occasionally display compositions of andesine or bytownite. (Figure 3 and see Supplementary data). Normal, inverse, and oscillatory zoning patterns are observed in some plagioclases, as indicated by variations in MgO, TiO_2, CaO, and An contents. As well as anorthite contents range between (An_{47-72}) from the core to the rim (see Supplementary data). Moreover, some of the plagioclase microphenocrysts and phenocrysts show sieve textures.

Pyroxenes are augite and diopsite based on Morimoto et al. (1988) (Figure 4a) and WinPyrox software Yavuz (2013). Mg≠ of the pyroxenes ranges between 64-85. Investigated pyroxenes exhibit normal, reverse and oscillatory zoning in terms of MgO, TiO_2, Cr_2O_3 and CaO (see Supplementary data). Reverse and oscillatory zoning within MgO -TiO_2 and Cr_2O_3 contents indicate reheating processes (magma mixing, new magma input and recharging) and mafic replenishment before the eruption (Gençoğlu Korkmaz, 2019; Ubide et al., 2014a;

2014b; 2014c). Using clinopyroxene-melt pairs that satisfy the conditions (Kd $_{Fe\text{-}Mg}$=0.27±0.03), yielding temperatures between 973 and 1080 °C and pressures ranging from 1 to 5.7 kbar. Temperature estimates for clinopyroxenes were also calculated according to Lindsley and Andersen (1983) (Figure 4b). When the clinopyroxenes were plotted on the pyroxene quadrilateral, the sample points aligned with isotherms between 950 and 1300 °C (Figure 4b). Although these values represent a broader temperature range, they generally align with the temperature values obtained Putirka (2008a), suggesting consistency.

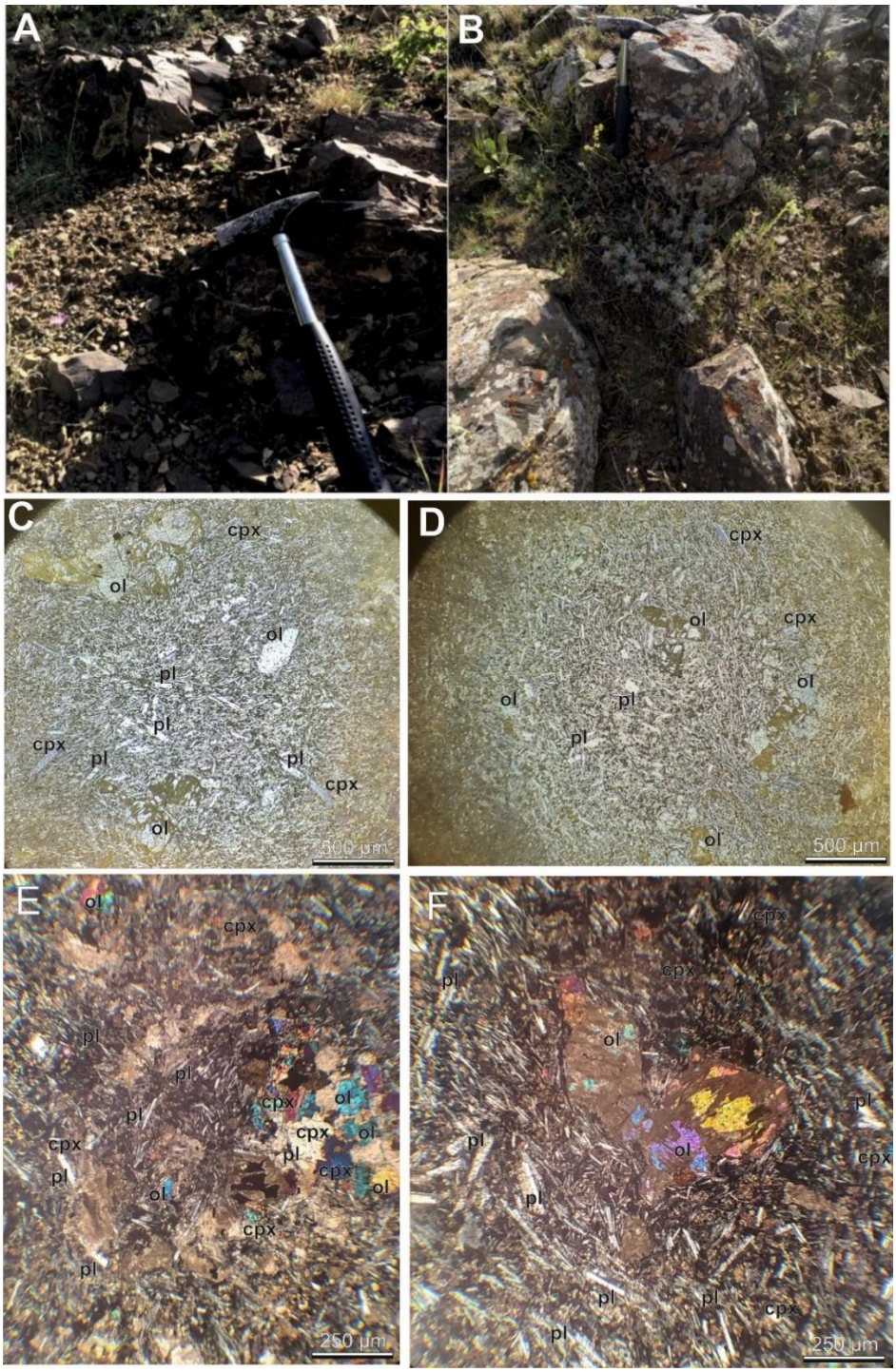

Figure 2. a), b) *Field appearance of the Tepekent basalts;* ***c), d), e), f)*** *Microphotographs of the investigated basalts. Mineral abbreviations are based on Whitney and Evans (2009)*

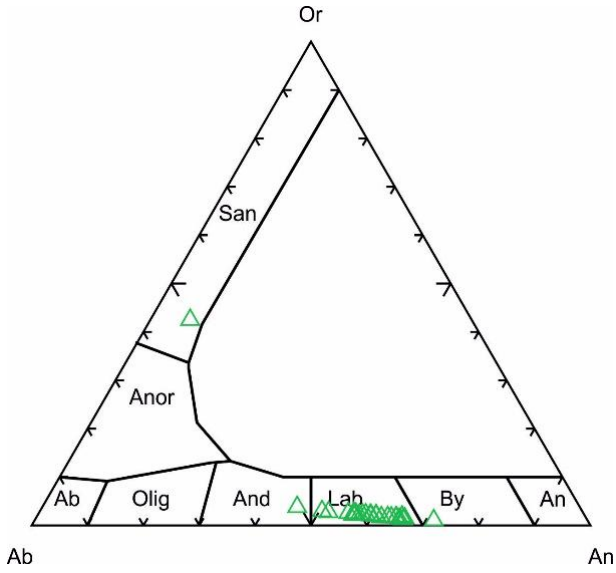

Figure 3. *Ab-An-Or classification diagram (Deer et al., 1963) of the feldspars from the investigated rocks.*

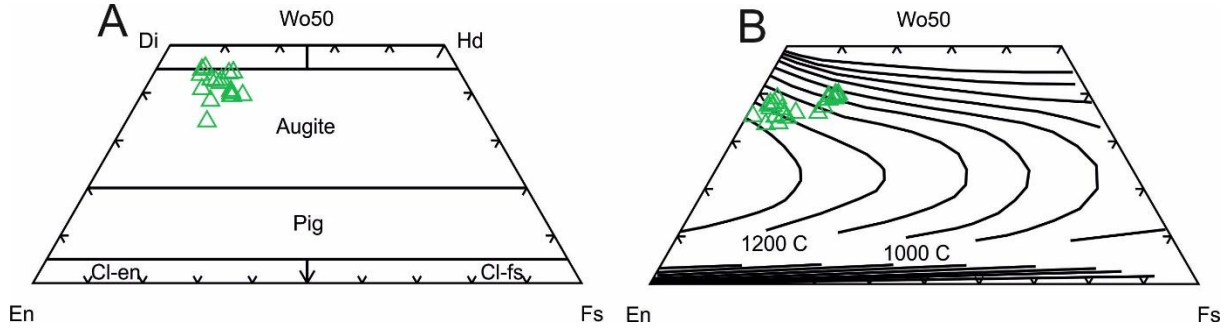

Figure 4. a) *Morimoto et al. (1988) pyroxene classification diagram and* ***b)*** *Crystallization temperatures based on Lindsley and Andersen (1983)*

Fo content [Fo = 100 × Mg/(Mg + Fe) in mol%] of the measured olivines ranges between 67-82. Major elements compositions were recorded in the olivine from the basalts: 0.001 to 0.014 wt%, Cr_2O_3; 0.16 to 0.5 wt%, CaO; 35-44 wt%, MgO. They are relatively homogeneous with Fo composition. Although many olivines in the same sample have been normal zoned in terms of Fo, some olivines have not displayed homogene distributions within Cr_2O_3, TiO_2 and CaO contents (see Supplementary data). Using olivine-melt pairs that satisfy the conditions (Kd Fe-Mg=0.30±0.03), the calculations were made for temperature values are around 1200°C.

3.2 Discussion

Chemical Relationship between the Miocene Basalts in the SVC

In the north-northwest of Konya, basaltic rocks are represented by a restricted basaltic sill or dike, which has previously been attributed to the Miocene-aged Sulutaş Volcanic Complex (Gençoğlu Korkmaz et al., 2017; Asan et al., 2021). In this study, the Tepekent basalts are examined alongside the previously reported Yükselen and Ulumuhsine basalts (Gençoğlu Korkmaz et al., 2017; Asan et al., 2021) to make correlation and perform the evaluation. The basaltic lavas in the Yukselen area, which outcrop over a restricted region, exhibit a distinct

whole-rock composition compared to the Ulumuhsine and Tepekent basalts. These lavas are alkaline basalts (Figure 5) and were previously classified as hawaiite-type sodic alkali basalts (Gençoğlu Korkmaz et al., 2017).

Silica versus major and trace element diagrams reveal a significant compositional distinction between the Yukselen hawaiites and the other basalts, with the former exhibiting a more mafic character. In contrast, no clear relationship indicating fractional crystallization (FC) is observed between the Ulumuhsine and Tepekent basalts (Figure 6 and 7). The major oxides and trace elements do not display homogeneous distributions, which suggests that the observed heterogeneity is better explained by assimilation-fractional crystallization (AFC) contamination processes rather than by FC alone (Figure 6 and 7). Nevertheless, certain trace elements, such as Zr, Yb, and Sr, exhibit similar concentrations across both basalt types, indicating underlying geochemical affinities.

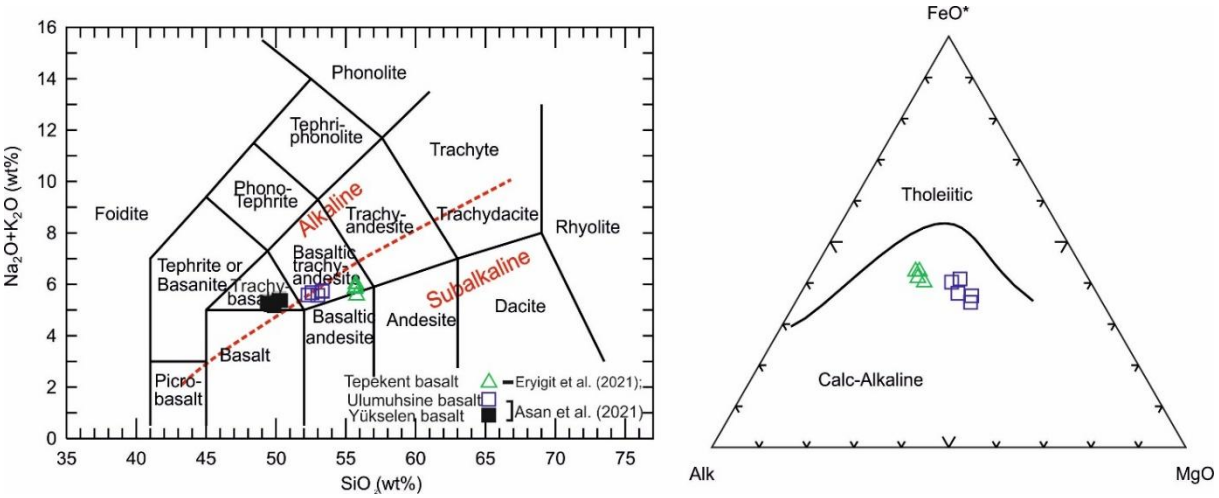

Figure 5. a) *Total alkali-silica (TAS) rock classification diagram based on Irvine and Baragar (1971) and* ***b)*** *AFM diagram for subalkaline rocks (Irvine and Baragar, 1971) Whole-rock geochemistry data of Tepekent basalts were taken from Eryiğit et al. (2022). The other basalts were taken from Asan et al. (2021)to correlate the Miocene?-aged basaltic rocks outcropped the N-NW of Konya*

Tectonic discrimination diagrams indicate that the Yükselen basalts display ocean island basalt (OIB) characteristics, whereas the Ulumuhsine and Tepekent basalts exhibit features consistent with enriched-mid-ocean ridge basalt (MORB) and crustal-contaminated arc basalts (Figure 8 and 9). The chondrite-normalized rare earth element (REE) diagram (Sun & McDonough, 1989) reveals a significant enrichment in light rare earth elements (LREEs), ranging from 20 to 200 times chondritic values. Notably, all three basalt types exhibit closely overlapping patterns, suggesting similar geochemical trends (Figure 8b).

As indicated by the diagrams (Figure 5-9), whole-rock geochemical data alone are insufficient to clearly distinguish calc-alkaline rocks outcropped around the investigated area. To address this limitation, this study incorporates mineral chemistry data and geostatistical interpretations to enhance the classification and understanding of petrogenetic processes.

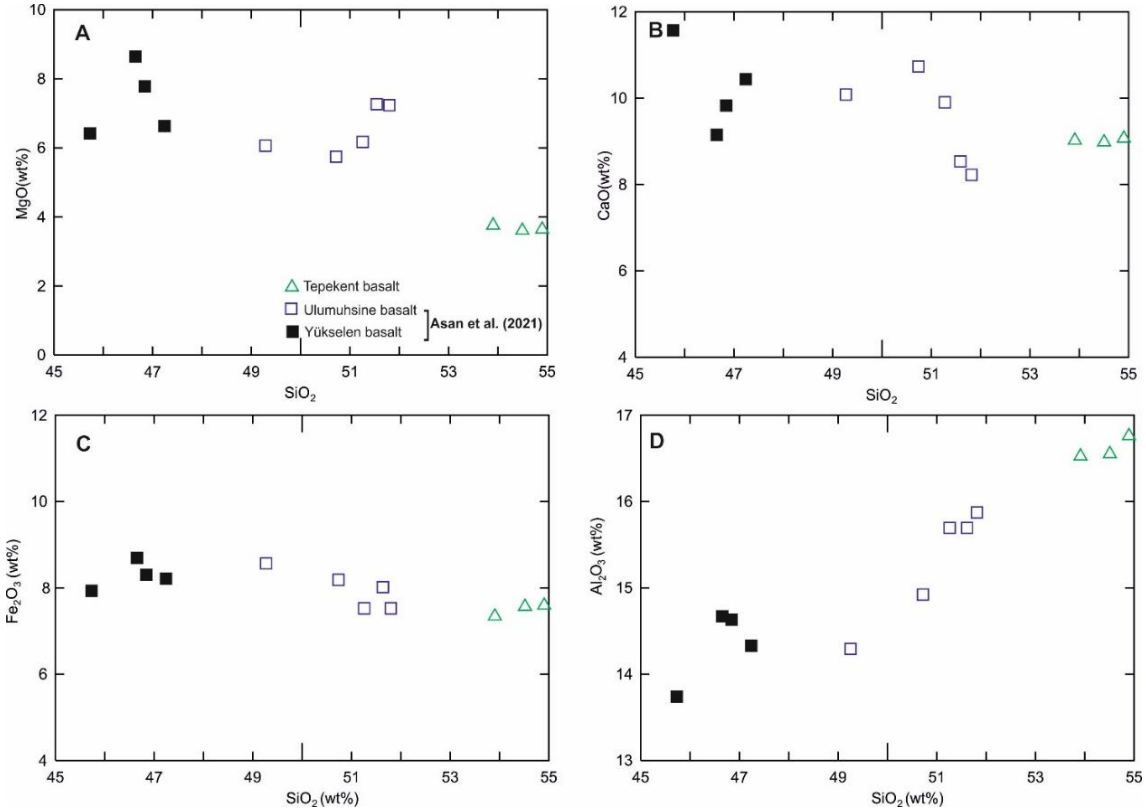

Figure 6. *Silica versus selected major oxide variation diagrams for investigated basalts. Whole-rock geochemistry data of Tepekent basalts were taken from Eryiğit et al. (2022). The other basalts were taken from Asan et al. (2021) to correlate the Miocene?-aged basaltic rocks outcropped the N-NW of Konya*

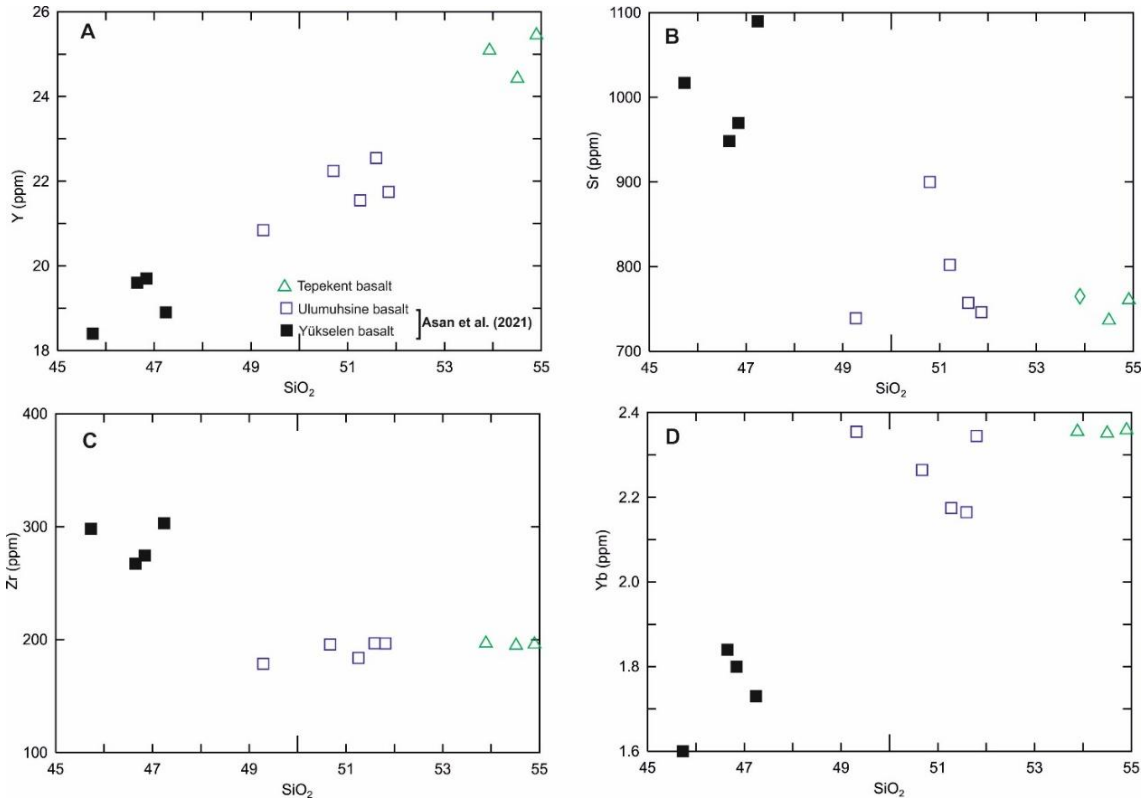

Figure 7. *Silica versus selected trace element variation diagrams for investigated basalts. Whole-rock geochemistry data of Tepekent basalts were taken from Eryiğit et al. (2022). The other basalts were taken from Asan et al. (2021) to correlate the Miocene?-aged basaltic rocks outcropped the N-NW of Konya*

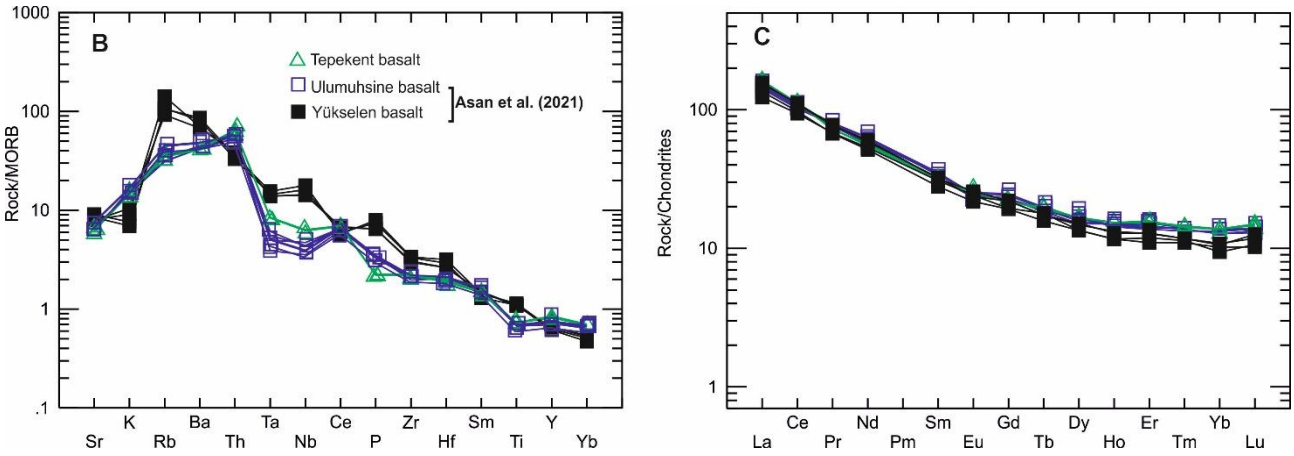

Figure 8. a) *MORB-normalized spider diagram (Pearce, 1983);* ***b)*** *Chondrite-normalized (Sun & McDonough, 1989) spider diagram for investigated rocks.*

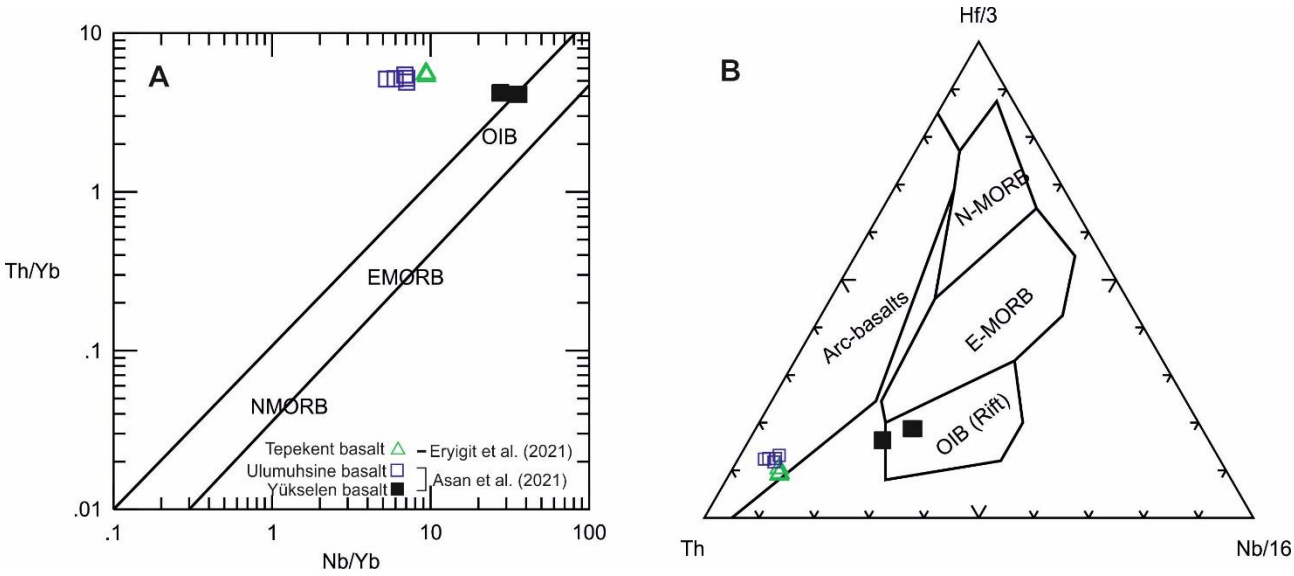

Figure 9. *Tectonic setting diagrams based on* ***a)*** *Pearce (2008) and* ***b)*** *Wood (1980)*

Complex Magma Chamber Process of the Tepekent Basalts

MnO, CaO and Cr_2O_3 compositions from the investigated olivines display nearly negative correlations with Mg≠ (Figure 10). The correlations of Mg≠ versus Cr_2O_3 and CaO align with fractional crystallization (Figure 10). In addition, olivine grains have CaO>0.1, indicating being phenocryst rather than mantle xenocryst (Thompson & Gibson, 2000; Gençoglu Korkmaz et al., 2019). However, the $Kd_{(Fe\text{-}Mg)}$ values of the olivines range from 0.105 to 0.204, which are lower than the expected $Kd_{(Fe\text{-}Mg)}$ equilibrium value of 0.29 ± 0.03, suggesting that they are not in equilibrium with their host liquid (Figure 11a). Some of the olivine grains are in equilibrium with the most mafic basalt from Ulumuhsine (Figure 11b Sample Y7, (Asan et al., 2021)). These olivines may be antecrysts, representing earlier solidified phases that were transported into the system during magma ascent.

The reverse and oscillatory zoning observed in pyroxene minerals, with respect to MgO, Cr_2O_3, and TiO_2 from the core to the rim, suggests that the magma has been replenished by a more mafic mantle source (Gençoğlu Korkmaz, 2019; Ubide et al., 2014a; 2014b; 2014c). Some of pyroxenes can share the similar chemical

properties (see Supplementary data). They can be antecrysts formed before eruption phase and cropped from the magma wall and transferred the system. Moreover, the oscillatory variations in An content and the presence of sieve and dusty textures in plagioclase further support this interpretation indicating instability and complex magmatic processes during crystallization (Streck et al., 2002; 2005; Ginibre & Wörner, 2007; Streck, 2008; Gençoğlu Korkmaz & Kurt, 2021).

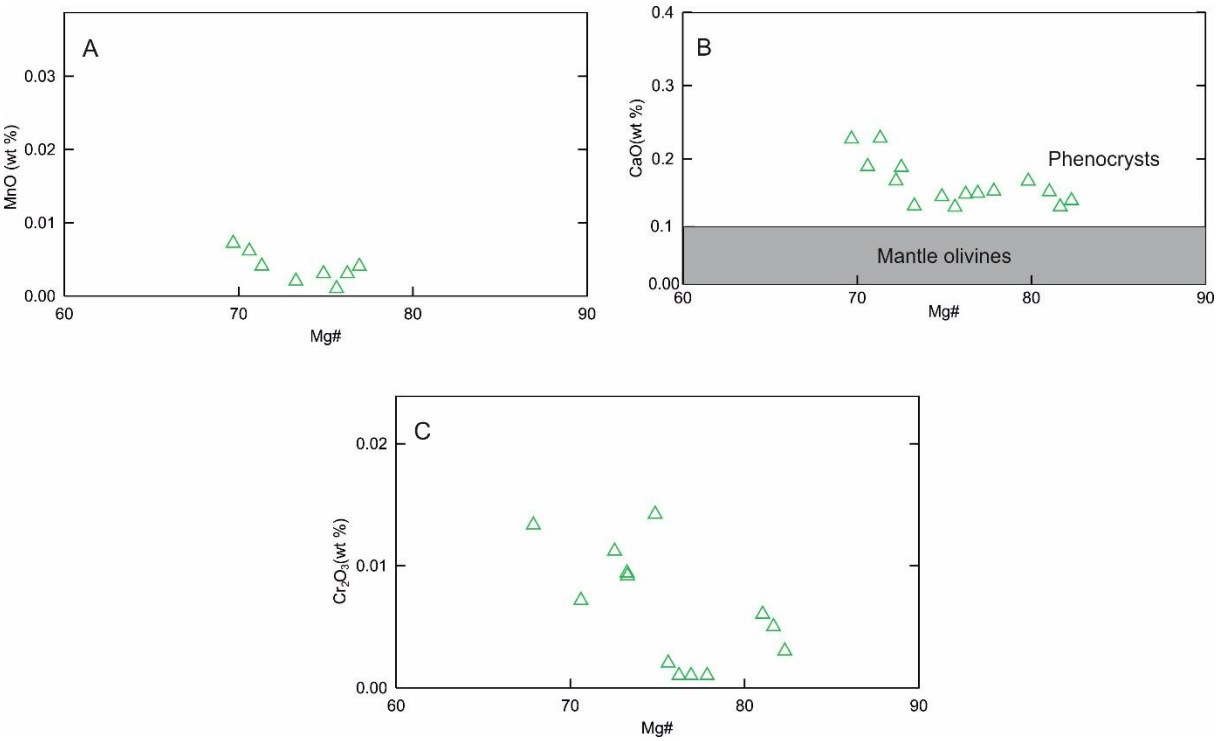

Figure 10. *Mg versus selected major oxide diagrams for investigated olivines*

Geostatistical Evaluation of the Basalts

In tephrochronology, occasionally Fe-Ti oxide pairs, biotite, amphibole, and pyroxene minerals are commonly used to correlate and associate tephra layers (Lowe, 2011). In this study, pyroxene minerals from the Tepekent basalts were specifically selected and utilized for correlation and classification purposes. To achieve this, classification and chemometric analyses, including PCA, UMAP, and k-medoids clustering, were performed.

Principal Component Analysis-PCA is a widely used linear dimensionality reduction method that transforms high-dimensional datasets into a lower-dimensional space while preserving as much variance as possible. It projects the data onto orthogonal axes, called principal components, which are aligned with the directions of maximum variance in the dataset. This method is particularly effective in datasets where variables are highly correlated, as it reduces redundancy by identifying uncorrelated linear combinations of the original features. PCA is often employed to simplify datasets for further analysis, including clustering and regression, by minimizing reconstruction error during the dimensionality reduction process (Jolliffe, 2002; Demšar et al., 2013). In volcanology, PCA has been applied to spatial and compositional data to differentiate volcanic units and interpret geochemical patterns (Prima & Yoshida, 2010; Mazzarini et al., 2016; Petrelli, 2021; Uslular et al., 2021).

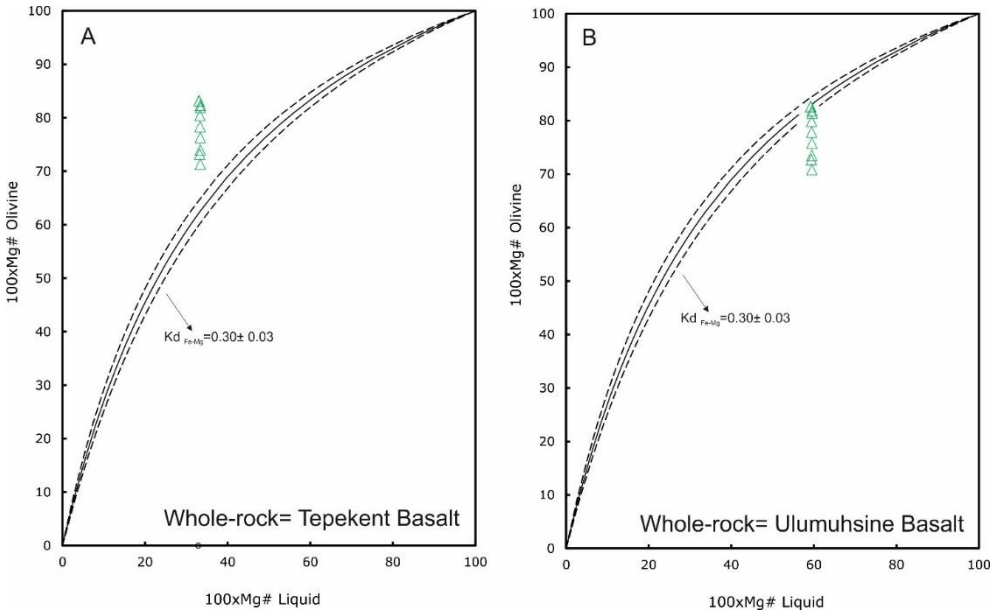

Figure 11. a) *Rhodes diagrams illustrating disequilibrium conditions between Tepekent basalts and the analyzed olivines.* ***b)*** *Rhodes diagrams indicating equilibrium conditions for the most mafic basalt from Ulumuhsine and a subset of the analyzed olivines. The equilibrium field for Fe/Mg exchange between olivine and basaltic melt ($Kd_{(Fe-Mg)} = 0.29 \pm 0.03$) is based on Matzen et al. (2011) and Putirka (2016)*

Uniform Manifold Approximation and Projection-UMAP is a nonlinear dimensionality reduction technique designed to preserve both global structure and local relationships in high-dimensional data. Unlike PCA, which relies on linear transformations, UMAP creates a low-dimensional manifold that retains the data's intrinsic topological properties. This makes UMAP particularly effective for datasets with nonlinear relationships, where preserving local neighborhoods is critical. UMAP has seen increased usage in Earth sciences for visualizing complex datasets, such as geochemical analyses of volcanic minerals, where its ability to distinguish subtle differences in composition is invaluable (McInnes et al., 2018; Becht et al., 2019). Moreover, k-medoids clustering is a robust partitioning algorithm that groups data into k-clusters using representative data points (medoids), which are actual data objects rather than centroids (Yousif & Yan, 2021). This method minimizes the sum of pairwise dissimilarities within each cluster, making it particularly effective in noisy or outlier-prone datasets (Yousif & Yan, 2021; Ren et al., 2022). It has significant applications across geosciences and biosciences, such as classifying fault systems, mineral assemblages, and spectral data in remote sensing, as well as clustering genomic sequences or ecological distributions. In tephrochronology, it can be used to classify volcanic ash layers and differentiate compositional variations in pyroclastic deposits by grouping similar geochemical signatures, aiding in the identification of volcanic sources and eruption dynamics. Clustering results obtained through k-medoids can be effectively visualized using UMAP, a nonlinear dimensionality reduction technique that preserves both global structure and local relationships in high-dimensional datasets. UMAP excels in representing the intrinsic topology of clusters, allowing clear differentiation of groups defined by k-medoids in a two- or three-dimensional space. To further validate and interpret clustering results, Principal Component Analysis (PCA) can be employed. PCA identifies the directions of maximum variance within the dataset, providing complementary insights into the overall structure

and confirming the robustness of the clustering. By combining k-medoids with UMAP for visualization and PCA for statistical verification, this approach offers a comprehensive framework for analyzing complex datasets. Such methodologies are particularly beneficial in fields like tephrochronology, where geochemical data of volcanic deposits can be clustered and visualized to discern compositional variations and eruption histories

The PCA and UMAP analyses of olivine minerals did not provide a clear distinction or correlation between the two calc-alkaline lava flows (Figure 12a and 12b). Investigated basalts and Ulumuhsine basalts can share common olivine grains or they can contain olivine grains within the similar composition. However, the PCA and UMAP diagrams and k-medoids clustering analysis (Table 1) for pyroxenes demonstrated a pronounced differentiation, suggesting that the two lava flows likely represent distinct magmatic events or magmatic episodes (Figure 13-14)**.**

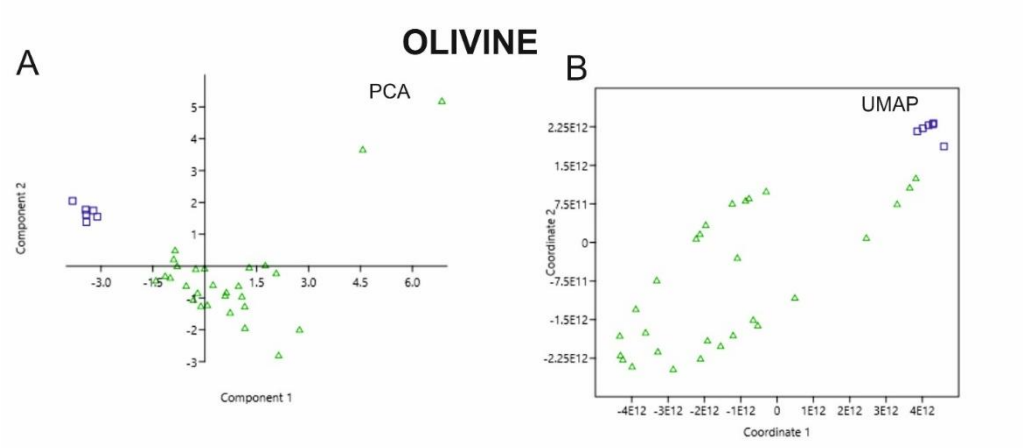

Figure 12. a) *Principal Component Analysis (PCA) and* ***b)*** *Uniform Manifold Approximation and Projection (UMAP) diagrams of the investigated olivines. Green triangles represent olivines from the Tepekent basalts, while blue squares denote those from the Ulumuhsine basalts. Olivine data for the Ulumuhsine basalts were taken from Asan et al. (2021). Despite the analysis, PCA and UMAP results were insufficient to effectively distinguish the basaltic lava flows based on olivine compositions.*

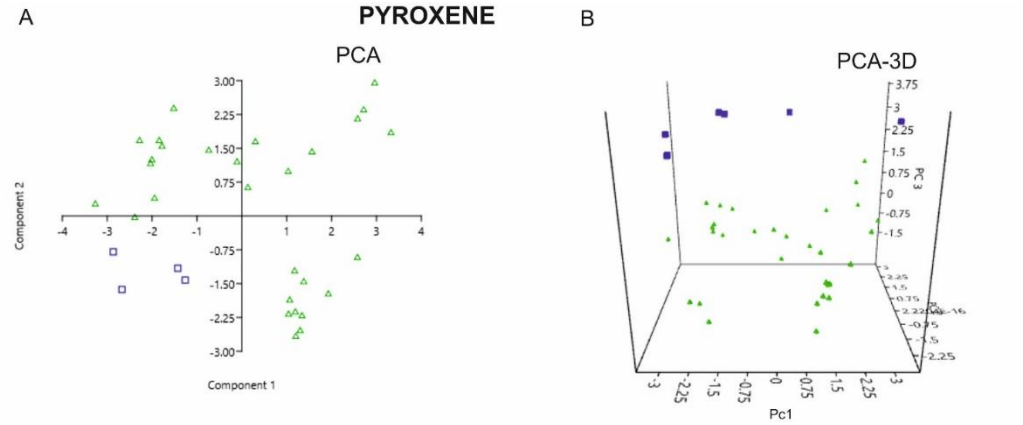

Figure 13. *PCA diagrams of the investigated pyroxenes and pyroxenes from Ulumuhsine basalts. Green triangles represent clinopyroxenes from the Tepekent basalts, while blue squares denote those from the Ulumuhsine basalts. Clinopyroxene data for the Ulumuhsine basalts were taken from Asan et al. (2021)*

Table 1. *K-medoids clustering analysis for pyroxenes*

k-medoids			
Item	Cluster	Item	Cluster
BT43/C1-1/1	1	BT44/C2/3	1
BT43/C1-1/2	1	BT44/C2/4	1
BT43/C1-1/3	1	BT44/C2/5	1
BT43/C2-1/1	2	BT44/C2/6	1
BT43/C2-1/2	1	BT44/C2/7	1
BT43/C2-1/3	1	BT43/C3-1/1	1
BT43/C2-1/4	1	BT43/C3-1/2	1
BT43/C2-1/5	1	BT43/C3-1/3	1
BT43/C2-1/6	1	BT44/C3/3	1
BT43/C5-1/1	1	BT44/C3/4	1
BT43/C5-1/2	1	BT44/C3/5	1
BT43/C5-1/3	2	BT44/C3/6	1
BT43/C5-1/4	1	*G-21B-1-px-5	2
BT43/C5-1/5	1	*G-21B-2-px6	2
BT44/C1-1/1	1	*G-21B-3-px-7a	2
BT44/C1-1/2	1	*G-21B-3-px-7b	2
BT44/C1-1/3	1	*G-21B-4-px-8a	2
BT44/C2/1	2	*G-21B-4-px-8b	2
BT44/C2/2	1		

* Sample data were taken from Asan et al. (2021).

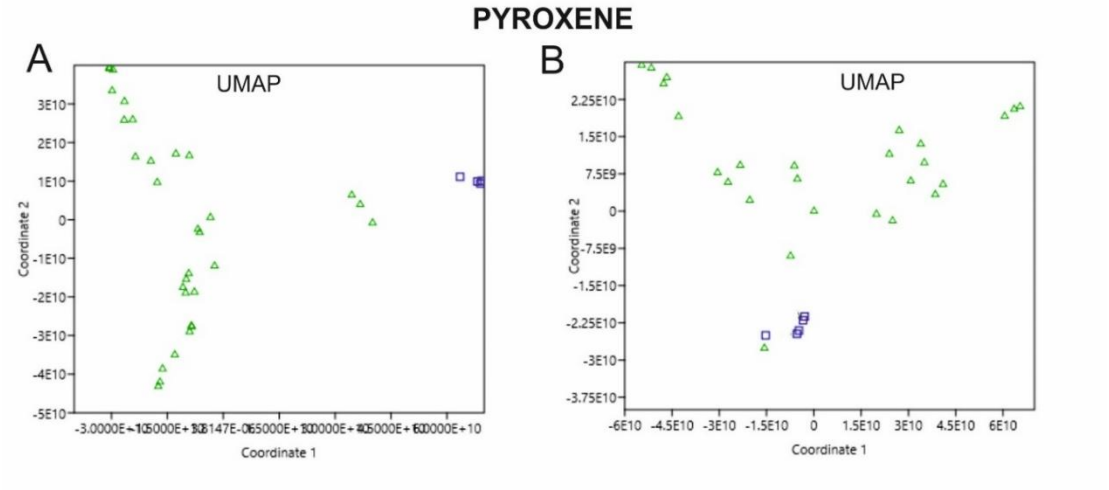

Figure 14. a) *UMAP (nonlinear, Euclidean distance) and* ***b)*** *UMAP (nonlinear, Bray-Curtis dissimilarity) visualizations of the investigated clinopyroxenes (green triangles) and clinopyroxenes from Ulumuhsine basalts (blue squares). The diagrams display the results of k-medoids clustering analysis, illustrating group separations based on compositional variations. These UMAP projections highlight how different distance metrics influence the clustering outcomes and the visualization of data relationships.*

4. CONCLUSION

This study underscores the efficacy of geostatistical interpretations of mineral chemistry in distinguishing between rocks with similar whole-rock geochemical characteristics, where bulk chemistry alone proves insufficient. Minerals such as Fe-Ti oxide pairs, amphibole, biotite, and pyroxene minerals play a critical role in tephrochronology for differentiating volcanic deposits. In this study, advanced geostatistical techniques, including Principal Component Analysis (PCA) and Uniform Manifold Approximation and Projection (UMAP), were applied to mineral chemistry data. PCA, a linear dimensionality reduction method, and UMAP, a nonlinear ordination technique, both proved instrumental in identifying subtle compositional differences between basaltic units with overlapping bulk compositions.

The Ulumuhsine and Tepekent basalts, despite their comparable whole-rock geochemical profiles, exhibit distinct pyroxene types based on mineral chemistry analyses. Notably, some olivines in the Tepekent basalts exhibit geochemical characteristics similar to those in the Ulumuhsine basalts. This resemblance suggests that these olivines may be antecrysts—minerals formed during earlier magmatic stages—that were incorporated into the Tepekent basalts during magma ascent through a complex magmatic plumbing system. This incorporation highlights the dynamic and multi-stage nature of magma evolution in the region. These differences suggest that the basalts are not products of the same lava flow and likely represent distinct basaltic products exposed different magmatic processes during their evolution. While mineral chemistry strongly supports this distinction, further geochronological and isotopic studies are necessary to confirm whether these basalts share a common origin or belong to the same eruptive episode.

This study emphasizes the value of combining mineral chemistry with both linear (PCA) and nonlinear (UMAP) ordination techniques to improve volcanic stratigraphy resolution. Such an approach provides a deeper understanding of magma evolution, particularly in cases where whole-rock geochemistry alone cannot adequately resolve genetic relationships between volcanic units.

ACKNOWLEDGEMENT

The author thanks Prof. Dr. Yusuf Kağan Kadıoğlu and Assoc. Prof. Dr. Kıymet Deniz for EPMA analysis.

CONFLICT OF INTEREST

The author declares no conflict of interest.

REFERENCES

Asan, K., Kurt, H., Gündüz, M., Gençoğlu Korkmaz, G., & Morgan, G. (2021) Geology, geochronology, and geochemistry of the Miocene Sulutas volcanic complex, Konya-Central Anatolia: genesis of orogenic and anorogenic rock associations in an extensional geodynamic setting. *International Geology Review*, 1-32.

Aydar, E., & Gourgaud, A. (1998) The geology of Mount Hasan stratovolcano, central Anatolia, Turkey. *Journal of Volcanology and Geothermal Research, 85*, 129-152.

Becht, E., McInnes, L., Healy, J., Dutertre, C.-A., Kwok, I.W., Ng, L.G., Ginhoux, F., & Newell, E.W. (2019) Dimensionality reduction for visualizing single-cell data using UMAP. Nature biotechnology 37, 38-44.

Best, M.G. (2003) Igneous and metamorphic petrology, 2 ed. John Wiley & Sons.

Biryol, C.B., Beck, S.L., Zandt, G., & Özacar, A.A. (2011) Segmented African lithosphere beneath the Anatolian region inferred from teleseismic P-wave tomography. Geophysical Journal International 184, 1037-1057.

Carr, M. (1990) IGPET 3.0. Unpublished manual.—Terra Sofia, Somerset, New Jersey.

Deer, W.A., Howie, R.A., & Zussman, J. (1963) Rock-forming Minerals: Vol. 4: Framework Silicates. Longman.

Delph, J.R., Biryol, C.B., Beck, S.L., Zandt, G., & Ward, K.M. (2015) Shear wave velocity structure of the Anatolian Plate: anomalously slow crust in southwestern Turkey. Geophysical Journal International 202, 261-276.

Demšar, U., Harris, P., Brunsdon, C., Fotheringham, A.S., & McLoone, S. (2013) Principal component analysis on spatial data: an overview. Annals of the Association of American Geographers 103, 106-128.

Deniel, C., Aydar, E., & Gourgaud, A. (1998) The Hasan Dagi stratovolcano Central Anatolia, Turkey evolution from calc-alkaline to alkaline magmatism in a collision zone. Journal of Volcanology and Geothermal Research 87 275-302.

Deniz, K., & Kadıoğlu, Y.K. (2019) Investigation of feldspar raw material potential of alkali feldspar granites and alkali feldspar syenites within Central Anatolia. Maden Tetkik ve Arama Dergisi 158, 265-289.

Eryiğit, B., Kurt, H., Asan, K., & Korkmaz, G.G. (2022) Petrography, Geochemistry, and Petrology of Volcanic Rocks in the Tepekent Region (Konya-Central Anatolia). Konya Journal of Engineering Sciences 10, 1002-1018.

Gençoğlu Korkmaz, G. (2019) The Origin of the Enclaves in Emirgazi (Konya) and its Surrounding Volcanites and Their Petrological Importance in the Genesis of the Regional Volcanism Konya Technical University Graduate Education Institute. Konya Technical University (in Turkish), p. 321.

Gençoğlu Korkmaz, G., Asan, K., Kurt, H., & Morgan, G. (2017) 40Ar/39Ar geochronology, elemental and Sr-Nd-Pb isotope geochemistry of the Neogene bimodal volcanism in the Yükselen area, NW Konya (Central Anatolia, Turkey). Journal of African Earth Sciences 129, 427-444.

Gencoglu Korkmaz, G., & Kurt, H. (2024) Complex Magma Chamber Dynamics and Volcanic Activity in the Karapınar Volcanic Field: Insights from Mineral and Whole-Rock Chemistry – A Review, in: Dr. Károly, N. (Ed.), A Comprehensive Study of Volcanic Phenomena. IntechOpen, Rijeka, p. Ch. 0.

Gençoğlu Korkmaz, G., & Kurt, H. (2021) Interpretation of the Magma Chamber Processes with the help of Textural Stratigraphy of the Plagioclases (Konya-Central Anatolia). European Journal of Science and Technology, 222-237.

Gencoglu Korkmaz, G., Kurt, H., & Asan, K. (2019) Origin Of Olivines From The Karapınar-Karacadağ Volcanic Complex (Central Anatolia), in: KALIPCI, A.P.D.E. (Ed.), 4. International Conference on Civil, Environmental, Geology and Mining Engineering, Nevşehir, pp. 269-275.

Gencoğlu Korkmaz, G., Kurt, H., Asan, K., & Leybourne, M. (2022) Ar-Ar Geochronology and Sr-Nd-Pb-O Isotopic Systematics of the Post-collisional Volcanic Rocks from the Karapinar-Karacadag Area (Central Anatolia, Turkey): An Alternative Model for Orogenic Geochemical Signature in Sodic Alkali Basalts. Journal of Geosciences 67, 53-69.

Ginibre, C., & Wörner, G. (2007) Variable parent magmas and recharge regimes of the Parinacota magma system (N. Chile) revealed by Fe, Mg and Sr zoning in plagioclase. Lithos 98, 118-140.

Irvine, T., & Baragar, W.R.A. (1971) A Guide to the Chemical Classification of the Common Volcanic Rocks. Canadian Journal of Earth Sciences 8, 523-548.

Jolliffe, I.T. (2002) Principal component analysis for special types of data. Springer.

Lindsley, D.H., & Andersen, D.J. (1983) A two-pyroxene thermometer. Journal of Geophysical Research: Solid Earth 88, A887-A906.

Lowe, D.J. (2011) Tephrochronology and its application: a review. Quaternary Geochronology 6, 107-153.

Matzen, A.K., Baker, M.B., Beckett, J.R., & Stolper, E.M. (2011) Fe–Mg partitioning between olivine and high-magnesian melts and the nature of Hawaiian parental liquids. Journal of Petrology 52, 1243-1263.

Mazzarini, F., Le Corvec, N., Isola, I., & Favalli, M. (2016) Volcanic field elongation, vent distribution, and tectonic evolution of a continental rift: The Main Ethiopian Rift example. Geosphere 12, 706-720.

McInnes, L., Healy, J., & Melville, J. (2018) Umap: Uniform manifold approximation and projection for dimension reduction. arXiv preprint arXiv:1802.03426.

Morimoto, N., Fabries, J., Ferguson, A.K., Ginzburg, I.V., Ross, M., Seifert, F.A., Zussman, J., Aoki, K., & Gottardi, G. (1988) Nomenclature of pyroxenes. American Mineralogist 73, 1123-1133.

Neave, D.A., & Putirka, K.D. (2017) A new clinopyroxene-liquid barometer, and implications for magma storage pressures under Icelandic rift zones. American Mineralogist 102, 777-794.

Pearce, J.A. (1983) Role of the sub-continental lithosphere in magma genesis at active continental margin. Continental Basalts and Mantle Xenoliths, 230-249.

Pearce, J.A. (2008) Geochemical fingerprinting of oceanic basalts with applications to ophiolite classification and the search for Archean oceanic crust. Lithos 100, 14-48.

Pecerillo, A. (2005) Plio-Quaternary Volcanism in Italy: Petrology, Geochemistry, Geodynamics. . 370.

Petrelli, M. (2021) Introduction to python in earth science data analysis: from descriptive statistics to machine learning. Springer Nature.

Prima, O.D.A., & Yoshida, T. (2010) Characterization of volcanic geomorphology and geology by slope and topographic openness. Geomorphology 118, 22-32.

Putirka, K.D. (2008a) Clinopyroxene thermobarometers.

Putirka, K.D. (2008b) Thermometers and Barometers for Volcanic Systems. Reviews in Mineralogy & Geochemistry 69, 61-120.

Putirka, K.D. (2016) Special Collection: Olivine: Rates and styles of planetary cooling on Earth, Moon, Mars, and Vesta, using new models for oxygen fugacity, ferric-ferrous ratios, olivine-liquid Fe-Mg exchange, and mantle potential temperature. American Mineralogist 101, 819-840.

Ren, J., Hua, K., & Cao, Y. (2022) Global optimal k-medoids clustering of one million samples. Advances in Neural Information Processing Systems 35, 982-994.

Şengör, A.C. (1979) Mid-Mesozoic closure of Permo–Triassic Tethys and its implications. Nature 279, 590-593.

Şengör, A.M.C., & Yılmaz, Y. (1981) Tethyan evolution of Turkey: A plate tectonic approach. Tectonophysics 75, 181-241.

Streck, M.J., Dungan, M.A., Malavassi, E., Reagan, M.K., & Bussy, F. (2002) The role of basalt replenishment in the generation of basaltic andesites of the ongoing activity at Arenal volcano, Costa Rica: evidence from clinopyroxene and spinel. Bulletin of Volcanology 64, 316-327.

Streck, M.J., Dungan, M.A., Bussy, F., & Malavassi, E. (2005) Mineral inventory of continuously erupting basaltic andesites at Arenal volcano, Costa Rica: implications for interpreting monotonous, crystal-rich, mafic arc stratigraphies. Journal of Volcanology and Geothermal Research 140, 133-155.

Streck, M.J. (2008) Mineral Textures and Zoning as Evidence for Open System Processes. Reviews in Mineralogy and Geochemistry 69, 595-622.

Sun, S., & McDonough, W. (1989) Chemical and isotopic systematics of oceanic basalts: implications for mantle composition and processes. Geological Society, London, Special Publications 42, 313-345.

Thompson, R.N., & Gibson, S.A. (2000) Transient high temperatures in mantle plume heads inferred from magnesian olivines in Phanerozoic picrites. Nature 407, 502.

Ubide, T., Galé, C., Arranz, E., Lago, M., & Larrea, P. (2014a) Clinopyroxene and amphibole crystal populations in a lamprophyre sill from the Catalonian Coastal Ranges (NE Spain): A record of magma history and a window to mineral-melt partitioning. Lithos 184-187, 225-242.

Ubide, T., Galé, C., Larrea, P., Arranz, E., & Lago, M. (2014b) Antecrysts and their effect on rock compositions: The Cretaceous lamprophyre suite in the Catalonian Coastal Ranges (NE Spain). Lithos 206-207, 214-233.

Ubide, T., Galé, C., Larrea, P., Arranz, E., Lago, M., & Tierz, P. (2014c) The Relevance of Crystal Transfer to Magma Mixing: a Case Study in Composite Dykes from the Central Pyrenees. Journal of Petrology 55, 1535-1559.

Uslular, G., & Gençalioğlu-Kuşcu, G. (2019) Mantle source heterogeneity in monogenetic basaltic systems: A case study of Eğrikuyu monogenetic field (Central Anatolia, Turkey). Geosphere 15, 29.

Uslular, G., Le Corvec, N., Mazzarini, F., Legrand, D., & Gençalioğlu-Kuşcu, G. (2021) Morphological and multivariate statistical analysis of quaternary monogenetic vents in the Central Anatolian Volcanic

Province (Turkey): Implications for the volcano-tectonic evolution. Journal of Volcanology and Geothermal Research, 107280.

Van Hinsbergen, D.J., Maffione, M., Plunder, A., Kaymakcı, N., Ganerød, M., Hendriks, B.W., Corfu, F., Gürer, D., de Gelder, G.I., & Peters, K. (2016) Tectonic evolution and paleogeography of the Kırşehir Block and the Central Anatolian Ophiolites, Turkey. Tectonics 35, 983-1014.

Weaver, B.L. (1991) Trace element evidence for the origin of ocean-island basalts. Geology 19, 123-126.

Whitney, D.L., & Evans, B.W. (2009) Abbreviations for names of rock-forming minerals. American Mineralogist 95, 185-187.

Wood, D.A. (1980) The application of a ThHfTa diagram to problems of tectonomagmatic classification and to establishing the nature of crustal contamination of basaltic lavas of the British Tertiary Volcanic Province. Earth and Planetary Science Letters 50, 11-30.

Yavuz, F. (2013) WinPyrox: A Windows program for pyroxene calculation classification and thermobarometry†. American Mineralogist 98, 1338-1359.

Yavuz, F., & Yıldırım, D.K. (2018) A Windows program for pyroxene-liquid thermobarometry. Periodico di Mineralogia 87.

Yousif, S., & Yan, W. (2021) Application and evaluation of a K-Medoids-based shape clustering method for an articulated design space. Journal of Computational Design and Engineering 8, 935-948.